THERMALLY TUNABLE BAND GAPS IN ARCHITECTED METAMATERIAL STRUCTURES

BY

CHAITANYA NIMMAGADDA

THESIS

Submitted in partial fulfillment of the requirements
for the degree of Master of Science in Mechanical Engineering
in the Graduate College of the
University of Illinois at Urbana-Champaign, 2018

Urbana, Illinois

Adviser:

Assistant Professor Kathryn Matlack

Abstract

The combined characteristics of periodicity and locally resonant features in metamaterial structures, or meta-structures, give rise to unique wave propagation characteristics such as relatively low and wide band gaps. These meta-structures have a fixed geometry and thus a fixed behavior, however applications that require structural vibration mitigation such as spacecraft and automotive components have variable vibration mitigation requirements over a range of operation and external conditions. In this work, we propose a method to thermally tune the band gaps of composite meta-structures, which combine a periodic lattice and locally-resonant inclusions, through changes in temperature of the structure. The concept primarily takes advantage of the different moduli of the two materials in the meta-structure that have drastically different temperature dependences, to preferentially tune the modulus of the lattice material compared to the resonant inclusion. We introduce an additional concept, termed thermal partitioning, to partially or fully open and close band gaps by locally controlling the temperature within the meta-structure. We demonstrate these results numerically with finite element simulations.

Acknowledgments

I would like to thank my advisor Prof. Kathryn Matlack for her unwavering support and guidance throughout my program. I am very fortunate to be a part of Wave Propagation and Metamaterials (WPM) Lab and I am grateful for her efforts in providing me with an opportunity to present and participate at a conference.

I would also like to thank Ignacio Arretche for all the technical discussions we used to have. I have had the pleasure to work alongside one of the finest graduate and undergraduate students at WPM Lab. Finally, I thank my family for their love and encouragement throughout.

Table of Contents

List of Figures

1 Introduction

Noise and vibrations create damaging conditions for structural components in spacecraft, aircraft, and vehicles, and can be a source of user discomfort and dissatisfaction. Typical strategies to mitigate noise and vibrations involve adding damping materials/treatments or active noise/vibration control devices a priori, which add mass to and increases the cost of the structure. An alternative is to redesign structural components as mechanical meta-structures, to embed the vibration mitigation properties directly into the component. These mechanical meta-structures are structured material that use meso-scale components to control wave propagation and vibration transmission. They incorporate concepts from phononic crystals and metamaterials to generate acoustic or elastic band gaps, or frequencies that cannot propagate [2–4]. Meta-structures are thus passively vibration immune in certain frequency ranges and can maintain load-bearing capabilities and desired static mechanical properties [5, 6].

In addition, constantly changing external conditions of structural components, such as a satellite launch vehicle during liftoff through the atmosphere or the combustion cycle of an automotive engine, cause variable vibration characteristics that need to be mitigated. One way to address this engineering challenge is to develop a structure whose properties adapt to external conditions such as deformation, applied load, applied temperature, and/or humidity. This concept of tunable metamaterials or phononic crystals has been explored in recent literature using deformations [7–9], applied loads [10], temperature-sensitive materials [11–15], topological transformation of structures [16–18], applied voltage to control the thickness and tension in elastomers [19, 20], magneto-granular materials [21] and magnetoelastic mate-

rials [22, 23]. While prior work has shown the ability to open, close, and generally tune band gaps with a variety of mechanisms, we instead focus on a method to tune the band gaps in a specified direction by analyzing the mode shapes of the meta-structure, given the ability to tune the modulus of the meta-structure constituents with an applied temperature.

In this work, we explore the idea of using temperature as an independent variable to tune the band gaps of 3D multi-material meta-structures that consist of a periodic lattice and locally resonant inclusions, with periodicity in one dimension. Recent work has shown that this combination of meso-structures in addition to the multi-material nature enables the formation of low and wide band gaps [1]. The coupling of the polycarbonate lattice and the steel resonators enabled band gap engineering through small manipulations of the lattice geometry, however these meta-structures have a fixed response once the geometry is set. In the present work, we exploit the temperature-dependent modulus of the lattice material to demonstrate how to tune the resonator modes and thus the band gaps of these meta-structures with an applied change in temperature of the structure.

The main goal of this work is to present a method to tune band gaps of a meta-structure by exploiting an activated change in material modulus. We present these ideas using a meta-structure whose materials moduli can be tuned with an applied temperature, however these concepts can readily apply to meta-structures of other materials that have tunable moduli (e.g. shape memory alloys, or magneto-elastic materials). To explain these ideas, we study a meta-structure with a polycarbonate lattice and a steel interior cube (the resonator) (Fig. 1), that has been previously studied elsewhere [1].

In this work, we first experimentally determine the temperature-dependent moduli of the chosen meta-structure constituents. We isolate the effects of the

temperature-dependent moduli and study how these changes influence the band gaps of the meta-structure. We subject this meta-structure to changes in temperature using finite element simulations that use experimentally-determined temperature-dependent material moduli. Dispersion relations of the meta-structure at different global temperatures show that the band gaps shift equally in the frequency spectrum, due to the thermally-induced moduli changes in the polycarbonate lattice. We introduce a concept called "thermal partitioning", where different sections of the structure are subjected to different temperatures. This allows us to tune the stiffness of certain band gap edge modes relative to others, resulting in partial or complete opening and closing of band gaps. We then numerically explore other effects of temperature on this specific meta-structure: thermal expansion and thermal stress effects. Finally, we numerically calculate vibration transmission through finite meta-structures with six unit cells to confirm the band gaps calculated in infinite meta-structures.

2 Temperature-dependent moduli of constituent materials

An increase in temperature will cause a decrease in the moduli of the meta-structure constituent materials, an expansion and distortion of the meta-structure geometry, and thermal stresses within the meta-structure. Here, we first isolate the effects of temperature-dependent moduli. The purpose is to gain insight into how to exploit temperature-dependent moduli to tune its vibrational properties (band gap frequency and width). We emphasize that the specific unit cell and the materials we study is a test case to illustrate these concepts, and is based on prior work that experimentally verified the band gap behavior of fixed-temperature meta-structures [1]. However, the idea and approach is applicable to other meta-structures whose lattice material has a tunable moduli.

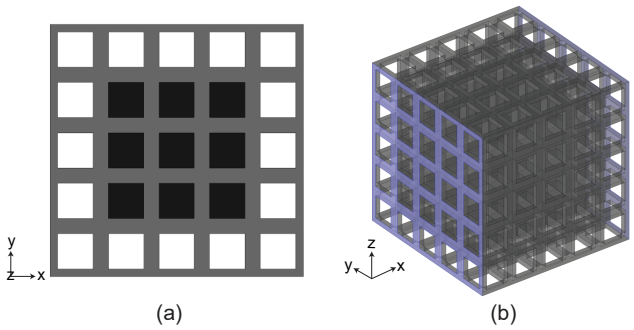

Figure 1: (a) Composite meta-structure cross section, containing steel resonator embedded in a polycarbonate cubic lattice. (b) 3D CAD model of meta-structure unit cell, with purple highlighted faces indicating periodic faces along x-direction.

We first measure the modulus of the constituent lattice material, polycarbonate, as a function of temperature. To do this, we use a Q800 Dynamic Mechanical Analysis (DMA) to interrogate standard samples of polycarbonate (dimensions 20mm x 5mm x 1mm) that were 3D printed using fused

deposition modeling (Stratasys Fortus 360mc), with long axis printed perpendicular to build direction. The moduli of the samples were measured using DMA in a tensile setup along the long axis of the sample, and we assume properties in the other two dimensions scale comparatively to the bulk material properties previously measured [1]. Three samples were subjected to increasing temperatures of $-140°C$ to $140°C$ at a frequency of 1Hz and heating rate of $2°C$/min, and the storage and loss modulus were measured at each temperature increment. This temperature range is selected based on the working temperature of the DMA and the glass transition temperature of the polycarbonate. Young's modulus was calculated by taking the square root of sum of squares of storage and loss modulus. The true modulus of the material is unknown. So, we use t-distribution with 95% confidence interval to come up with an estimate of the range in which the true modulus will lie. The calculations involved are shown as follows,

$$\overline{E} = \frac{\sum_{i=1}^{N} E_i}{n} \tag{1}$$

$\overline{E}$ is the average modulus and n is the number of samples being tested. In this work three samples were tested, $n = 3$.

$$s^2 = \frac{\sum_{i=1}^{N} (E_i - \overline{E})^2}{n-1} \tag{2}$$

's' being the standard deviation.The estimate of the true modulus is given by

$$\overline{E} \pm \ s * t_{n-1,\alpha/2} / \sqrt{n} \tag{3}$$

For 95% confidence interval, α=1-0.95=0.05. In this particular case, $t_{2,0.025} = 4.3027$. The average Young's modulus (with standard deviation ranging from 0.027 GPa to 0.161 GPa) dependence on temperature is shown in Fig. 2 where the upper and lower bounds shown correspond to the 95% confidence interval. Young's modulus decreases over 54% with an increase in temperature from $-140°C$ to $140°C$, while the moduli of steel is comparatively constant over this temperature range (less than 6% change in moduli [24]).

Prior work on this meta-structure design indicated that the modal stiffness of the modes surrounding the band gaps was controlled by the lattice stiffness and the beams connecting the resonator to the surrounding structure [1]. In particular, the beams connecting the resonator to the surrounding lattice act under axial and bending deformation in a locally-resonant longitudinal mode that controls the lower edge of the band gap. Both the lattice effective stiffness and stiffness of the beams under axial or bending deformation are proportional to the Young's modulus of the bulk lattice material. Thus, we expect the measured modulus temperature dependence to cause a decrease in frequency of the meta-structure modes with an increase in temperature, resulting in a decrease in the band gap frequency.

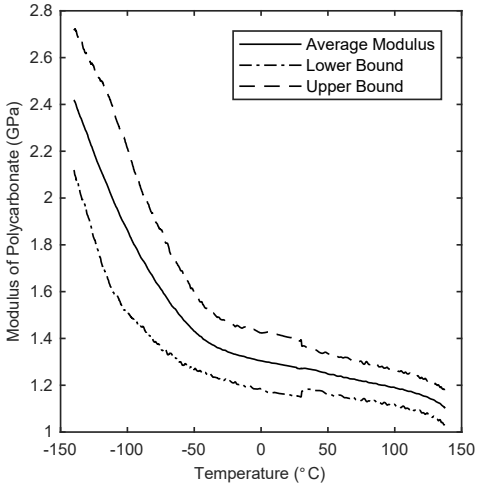

Figure 2: The modulus of 3D printed polycarbonate averaged over three samples as a function of temperature in the range $-140°C$ to $140°C$ using a DMA, and showing modulus bounds.

3 Thermal effects on band gaps in infinite meta-structures

3.1 Methods

To analyze the meta-structure's thermally-dependent vibrational response, we conduct finite element simulations on 3D meta-structures that are infinitely periodic in 1D using COMSOL Multiphysics. The polycarbonate material, when 3D printed, will be orthotropic. We thus model the polycarbonate material as orthotropic linearly elastic, using a scaling factor of 0.88 for the modulus along the build direction ($E_z = 0.88E_x$, $E_x = 1$ GPa) [1]. For simplicity, we assume the thermal expansion coefficient is isotropic, such that the modulus scaling factor remains constant at all applied temperatures. While the thermal expansion coefficient may in fact be orthotropic in 3D printed polycarbonate, this will likely only have a small influence on the behavior. We import the experimentally-determined temperature-dependent modulus of the polycarbonate measured in Sec. 2. The steel resonator is modeled as isotropic and linearly elastic, with a temperature-dependent modulus as a polynomial relation defined elsewhere [24] and extrapolated to the lower range of temperatures studied here (to $-140°C$). We analyze the polycarbonate-steel meta-structure at three different temperatures: $-140°C$, $20°C$ (room temperature), and $140°C$.

To calculate the dispersion relations, we solve the following thermal-mechanical boundary problem. We account for thermally-induced geometrical effects by first applying a change in temperature to the unit cell and allowing it to expand/contract. We impose boundary conditions on the faces with normal in the x-direction such that these faces remain flat (using a combination of

rigid connectors and a fixed connector), in order to apply periodic boundary conditions to calculate the dispersion curves and resulting band gaps. In COMSOL, thermal expansion can be applied by right clicking on the "Linear elastic material" under Solid Mechanics and choosing "Thermal Expansion". For free thermal expansion, right click on the boundary conditions to include thermal expansion on the faces. Select the option "Inherit from domain". This will allow completely free thermal expansion ensuring the faces in the periodic direction are flat. In Sec. 5, we validate this approach with simulations on finite meta-structures. The unit cell is otherwise free to expand or contract, and we account for this since a change in unit cell size will affect the frequency of the modes. The mismatch in thermal expansion coefficients between the polycarbonate and steel will cause a distortion of internal geometry and thermal stress at the interface between the two materials, however for the moment, we ignore these effects. In Sec. 4, we show the thermally-induced change in geometry has a negligible effect on the dispersion relations, but thermal stresses will likely affect the vibration behavior. We extract the deformed unit cell geometry and use this unit cell for the dispersion analysis. The density values should be updated owing to conservation of mass. For updated density values, the volume of the domains can be obtained by selecting the domains in the graphics window and clicking "measure" in the Geometry tab. We apply Floquet periodic boundary conditions on the periodic faces with normal in the x-direction (Fig. 1b), solve the eigenvalue problem at increasing values of the wavenumber along the periodic direction, and calculate the dispersion relations of the meta-structure in terms of frequency and wavenumber dependence.

3.2 Global Temperature Change: Dispersion Relations

The dispersion relations of the meta-structure with a globally applied temperature of $-140°C$, $20°C$, and $140°C$ are shown in Fig. 3. From an applied temperature of $20°C$ to $-140°C$, the lattice modulus increases from approximately 1.3 GPa to 2.4 GPa, causing the frequency of all modes to increase. The band gap width increases from 2,854 Hz to 3,934 Hz, the band gap center shifts from 8,560 Hz to 11,719 Hz, and the normalized band gap width slightly increases from 33.3% to 33.6%. If we only consider the change in moduli due to temperature and ignore the change in length of the unit cell, then the normalized band width remains constant. From an applied temperature of $20°C$ to $140°C$, the modulus decreases from approximately 1.3 GPa to 1.1 GPa. The decrease in modulus shifts all the modes downwards. The band gap width decreases from 2,854 Hz to 2,631 Hz and the band gap center decreases from 8,560 Hz to 7,932 Hz. The normalized band gap width decreases slightly from 33.3% to 33.2%. These results show that an increase in modulus of the polycarbonate lattice due to a decrease in temperature causes a frequency increase of all the modes, and vice-versa. All the modes scale linearly in the frequency spectrum with this global change in temperature, which can be used to shift the band gaps up or down in the frequency spectrum. We can use this technique effectively to tune the range of forbidden frequencies.

3.3 Thermal partitioning of the meta-structure

In the above simulations we change the applied temperature of the entire meta-structure uniformly. This causes the modes to shift equally in the frequency spectrum, resulting in a pure shift of the band gap and the normalized

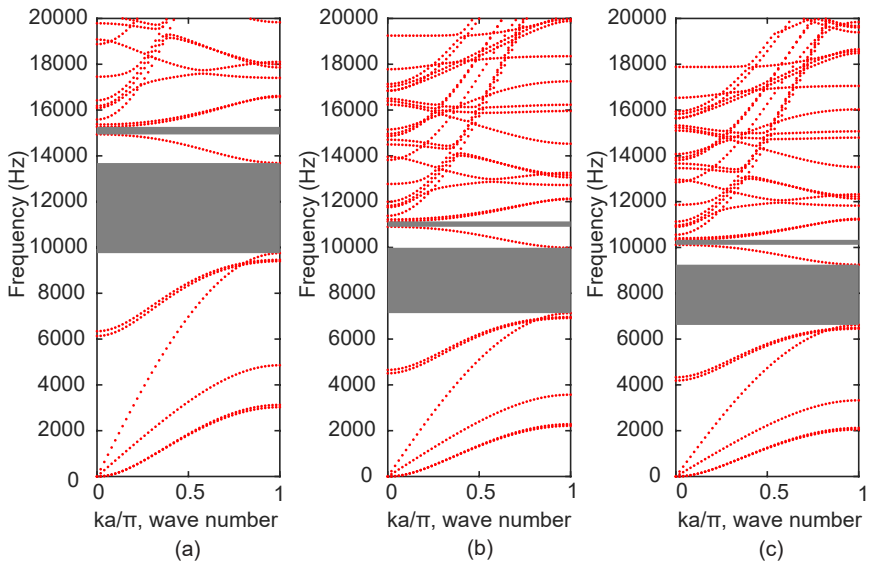

Figure 3: Dispersion curves of the meta-structure with temperature-dependent PC modulus at a) $-140°C$, b) $20°C$, and c) $140°C$.

band gap width remains exactly constant. To control individual modes relative to other modes and thus change the normalized width of the band gaps, we introduce a new concept called thermal partitioning. In this concept, we partition the lattice of the meta-structure into different domains (e.g. certain beams, lattice frame, resonator coating) and subject each set of domains to different thermal boundary conditions. This could be accomplished through carefully controlled heat flux through the sample, or by resistive elements 3D printed into the lattice structure. Maintaining sharp temperature differences locally may present a bigger challenge. The idea behind this step is that different portions of the lattice contribute different amounts to the modal stiffness and thus frequency of each mode. By spatially controlling the applied temperature, we bring about local changes in the modulus, which can independently control the stiffness of some modes relative to other modes.

We apply this thermal partitioning concept to tune the width of both the first and second band gaps of the meta-structure. To do this, we first analyze

the mode shapes of the modes surrounding the band gap, then identify a set of beams in the lattice that have a higher contribution to modal stiffness of one of those modes. We initially approximate this by visually depicting which beams in the unit cell deform the most, and we then quantify this by calculating the modal strain energy contributions of this set of beams. Modal strain energy is commonly used to quantify how strongly different elements contribute to the modal stiffness for damage localization in structures [25–27].

The modal elastic strain energy, E_i^j, of domain j of the i^{th} mode can be written as:

$$E_i^j = \frac{1}{2} \left\{U_i^j\right\}^T \left[K^j\right] \left\{U_i^j\right\} \tag{4}$$

where K^j is the local stiffness matrix of domain j, and U_i^j is the displacement vector of domain j in the i^{th} mode. When we measure the modal strain energy of a single mode, U_i can be written as an arbitrary constant, c, times the eigenvector, ϕ_i, of the corresponding mode. The modal strain energy can now be written as:

$$E_i^j = \frac{1}{2} c^2 \left\{\phi_i^j\right\}^T \left[K^j\right] \left\{\phi_i^j\right\} = \frac{1}{2} c^2 K_i^j \tag{5}$$

where K_i^j is the modal stiffness contribution of domain j to the i^{th} mode. Modal strain energy is thus proportional to the modal stiffness of the structure. So by measuring the modal strain energy of individual beams or other

domains of the unit cell, we quantify the contribution of these respective domains to the overall modal stiffness. The total modal stiffness can be expressed as a sum over all domains of the unit cell,

$$K_i = \sum_{j=1}^{N} K_i^j \tag{6}$$

where N is the total number of domains of the meta-structure unit cell, and K_i^j is the contribution from j^{th} domain to the total modal stiffness, K_i. We define $\overline{K_i}^j$ as the normalized stiffness contribution of domain j of the total modal stiffness of mode i:

$$\overline{K_i}^j = \frac{K_i^j}{K_i} \tag{7}$$

We use this parameter $\overline{K}_i^j$ as a metric to determine which domains to thermal partition, and thus modulate the band gap. We then tune the temperature of those beams independently of the rest of the lattice. This results in one edge mode shifting in frequency more so than the other edge mode, resulting in a change in band gap width.

3.3.1 Tuning the first band gap

We first apply thermal partitioning to change the width of the first band gap. To understand which domains of the unit cell to partition, we consider the edge mode shapes of the first band gap. The upper edge mode of the band gap is a torsional mode, Fig. 4(b), where the out-of-plane beams (beams

perpendicular to the direction of periodicity) have a larger contribution to the modal stiffness compared to the lower edge mode, based on their relative modal strain energy contributions: the out-of-plane beams contribute to 3% of the strain energy of lower edge mode, but 21% of the strain energy of the upper edge mode. The corresponding pie chart depicting relative modal strain energies is shown in Fig. 5(b), 6(b). Thus, a change in modulus of the out-of-plane beams will preferential change the frequency of the upper edge mode while keeping the frequency of the lower edge mode roughly constant.

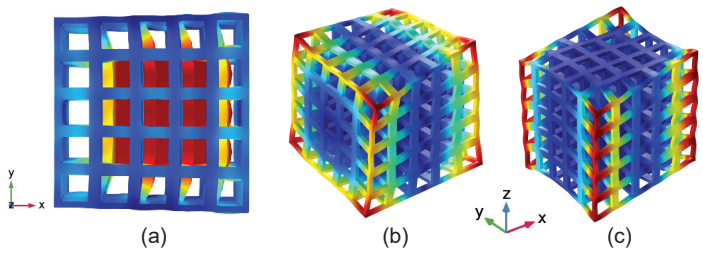

Figure 4: (a) Lower edge mode of the first band gap involves a mixture of longitudinal and flexural motion; b) upper edge mode of the first band gap (and lower edge mode of the second band gap) is a torsional mode; c) upper edge of the second band gap is a shear mode. 1D periodicity is in the x-direction.

The lower edge mode of this band gap is a combination of a longitudinal resonator mode along the direction of periodicity and a rotational resonator mode, as seen in Fig. 4(a) [1]. The in-plane beams (beams along the direction of periodicity) contribute more to the stiffness of the lower edge mode more than they contribute to the upper edge mode, as quantified by the modal strain energy distribution: the in-plane beams contribute 61% of the total strain energy of the lower edge mode, while the same beams contribute only 12% of the upper edge mode, Fig. 5(a), 6(a). This can also be understood as the in-plane beams are acting under axial deformation in this mode and the out-of-plane beams act under bending deformation, and beams are much

stiffer under axial deformation compared to bending. Thus, we expect that a modulus change of in-plane beams will cause a larger shift of the lower edge mode compared to the upper edge mode.

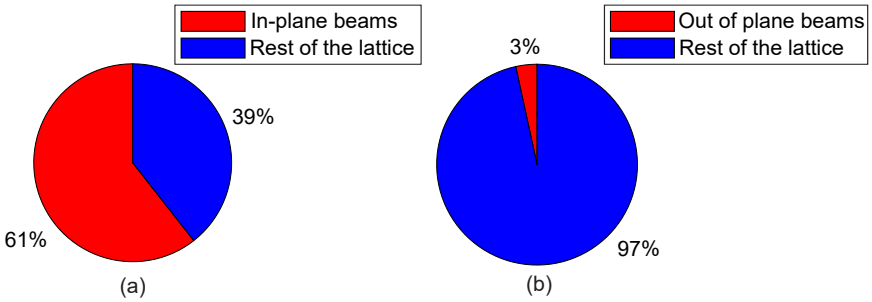

Figure 5: Relative strain energy contribution from (a) In-plane beams; b) Out of plane beams to the longitudinal mode, Fig. 4(a).

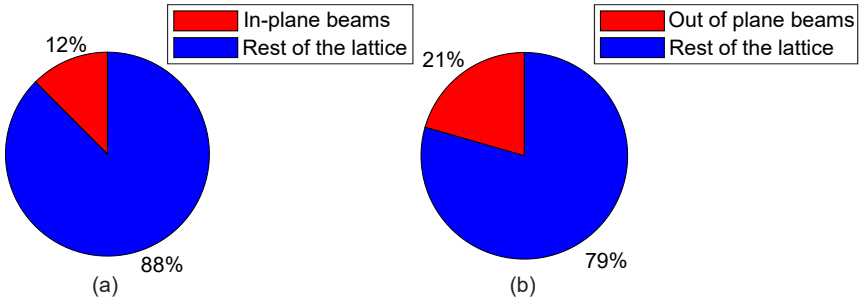

Figure 6: Relative strain energy contribution from (a) In-plane beams; b) Out of plane beams to the torsional mode, Fig. 4(b).

To study the effects of this thermal partitioning concept on the meta-structure band gaps, we choose to partition the unit cell in two different ways to preferentially shift the frequency of either the upper or lower band gap edge mode: (1) to tune the upper edge mode, we partition the lattice into a set of out-of-plane-beams and the remainder of the lattice, and (2) to tune the lower edge mode, we partition the lattice into a set of in-plane beams and the remainder of the lattice.

We first subject the out-of-plane beams (red) shown in Fig. 7(d) to a

temperature of $140°C$ and the rest of the lattice is held at $-140°C$. The dispersion curves for this configuration are shown in Fig. 7(c). We compare this to the dispersion curves where the entire meta-structure is subjected to $-140°C$, Fig. 7(a). The first band gap width has reduced by 990 Hz with the band gap center now at 11,117 Hz. As predicted, thermal partitioning in this case shifts the upper edge of the band gap downwards, decreasing the normalized bandwidth from 33.6% to 26.5%. By subjecting the out-of-plane beams to a higher temperature, we decrease the modulus of these beams, which results in a decrease in modal stiffness and thus frequency of the modes to which these beams contribute. The shift in lower edge of the first band gap is 107 Hz, whereas the upper edge decreased by 1,097 Hz, confirming these beams preferentially contribute to the modal stiffness of the upper edge mode compared to the lower edge mode. Thus, this approach of thermal partitioning gives us a way to shift one mode roughly independently of another, resulting in a change in band gap width.

To shift the upper edge of the band gap upwards, the out-of-plane beams (blue) are maintained at $-140°C$ while keeping the entire structure at $140°C$ as shown in Fig. 8(d). We compare the dispersion curve of this structure (Fig. 8(c)) to the dispersion curve where the entire meta-structure is subjected to $140°C$, Fig. 8(a). We now see that the upper mode of the first band gap moves up from 9,248 Hz to 9,879 Hz, whereas the lower mode is almost at the same frequency (6,617 Hz to 6,697 Hz). The normalized band width increases from 33.2% to 38.4%. A decrease in temperature of out-of-plane beams corresponds to an increase in modulus, which increases the frequency of the upper edge mode. This concept of thermal partitioning works in both directions: we can partially open and partially close band gaps.

Similarly, to tune the lower edge of the band gap, we subject the in-plane

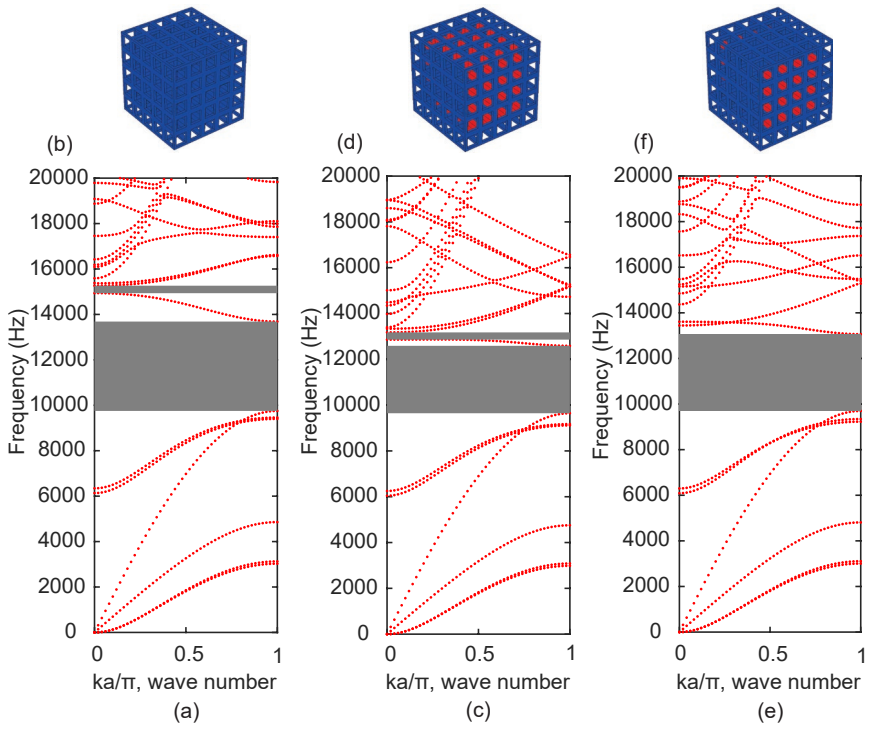

Figure 7: Results of thermal partitioning to decrease width of first band gap (c,d) and close the second band gap (e,f): (a) Reference meta-structure dispersion relation of unit cell (b) subjected to $-140°C$. (c) Dispersion relation of lattice subjected to thermal partitioning shown in (d), where out of plane beams (red) are subjected to $140°C$ and the rest of the lattice (blue) is subjected to $-140°C$. (e) Dispersion relation of lattice subjected to thermal partitioning shown in (f), where some out-of-plane beams (red) are subjected to $140°C$ and the rest of the lattice (blue) is subjected to $-140°C$.

beams to $-140°C$ and the rest of the lattice to a high temperature as seen in Fig. 8(f). When we compare the dispersion curves in Fig. 8(e) with that of the high temperature analogue, Fig. 8(a), we see that lower mode initially at 6,617 Hz increases to 8,086 Hz, decreasing the normalized band width from 33.2% to 17.2%, almost by half. The upper edge of the first band gap moves up slightly from 9,248 Hz to 9,611 Hz, because of the smaller contribution from the in-plane modes to the torsional modal stiffness compared to the longitudinal mode.

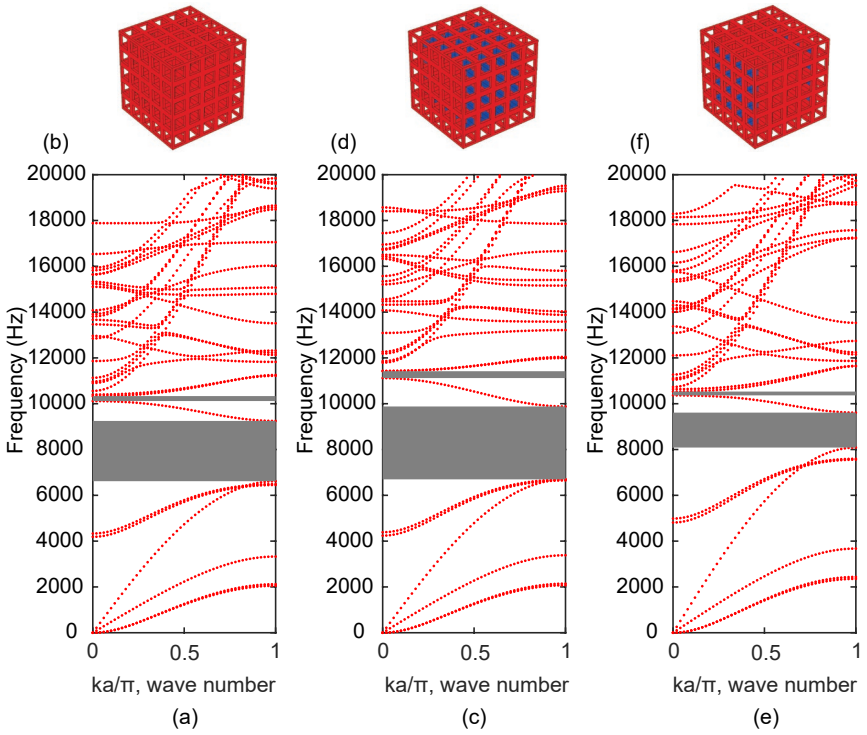

Figure 8: Results for thermal partitioning to increase (c,d) and decrease (e,f) the first band gap width: (a) Reference meta-structure dispersion relation of entire unit cell subjected to $140°C$ as in (b). Widening the band gap: (c) Dispersion relation of lattice subjected to thermal partitioning in (d), where out-of-plane beams (blue) are subjected to $-140°C$ and the rest of the lattice (red) is subjected to $140°C$. Narrowing the first band gap: (e) dispersion relation of lattice subjected to thermal partitioning in (f), where in-plane beams (blue) are subjected to $-140°C$ and the rest of the lattice (red) is subjected to $140°C$.

3.3.2 Tuning the second band gap

Thermal partitioning analysis can be applied to tune other band gaps of the meta-structure. For the second band gap, the lower and upper edge modes are shown in Fig. 4(b,c), respectively. The lower edge mode is a torsional mode and the upper edge mode is a shear mode, both with deformation concentrated in the lattice. Closing the second band gap can be achieved by moving the shear mode downwards or the torsional mode upwards. Here, we choose the former approach. The relative displacements of the out-of-plane

beams in the XZ plane are higher for the shear mode than the torsional mode. Starting from the condition where the entire structure is subjected to $-140°C$, we increase the temperature of one set of out-of-plane beams as shown in Fig. 7(f) to $140°C$. By increasing the applied temperature of these beams, the stiffness of the shear mode decreases. This causes the shear mode to decrease below the torsional mode, completely closing the band gap, Fig. 7(e).

3.3.3 Algorithm for thermal partitioning

In the prior section, we presented a method to shift the band gap width with thermal partitioning through a manual process. In order to maximize the band gap shift, we introduce a simple algorithm to find the optimal shift, given some discretization of the PC lattice. To do this, we discretize the unit cell into small domains: specifically, each of the individual 96 beams that connect the resonator to lattice, the external lattice frame, the resonator, and the resonator coating. We then define a vector, C_1, that contains the normalized modal strain energy contribution to mode 1 from each of these individual domains, where mode 1 is the lower edge of the band gap of interest. We define vector C_2 that contains the normalized modal strain energy contribution to mode 2 from each of the individual domains, where mode 2 is the upper edge of the band gap of interest. We aim to maximize (or minimize) vector $C_3 = C_2 - C_1$, to obtain the maximum difference in strain energy between the modes. This simply translates into selecting the domains that have a positive (or negative) value to shift mode 2 upwards relative to mode 1 (or mode 1 downwards relative to mode 2).

We use the built-in linear programming solver in MATLAB, "intlinprog", to optimize our domain space. To find the optimal configuration, we parametrize

the domains as binary variables. We then apply a change in temperature to the domains selected by the algorithm, i.e. those with value 1 at the end of the optimization process. Note in this approach, we assume the influence of one domain does not depend on whether other domains nearby are thermal partitioned.

We apply the thermal partitioning algorithm to the first band gap to find the optimal set of domains to partition. The optimal set includes the in-plane beams, just as we chose in the previous analysis (Fig. 8(f)), with the addition of the polycarbonate coating around the resonator, as shown in Fig. 9(d). This results in a minimum band width of 12.6% (Fig. 9(c)), as opposed to 17.2% that resulted from the manual process shown in Fig. 8(e). We also consider the complementary case of Fig. 9(d) in order to maximize the band gap. The first band gap width increases to 49.4% as seen in Fig. 10, much larger than the increase to 38.4% resulting from the manual process in Fig. 8c.

We then apply the algorithm to the second band gap. The optimal set of domains to thermal partition includes some out-of-plane beams as shown in Fig. 9(f). This is similar to our approximation studied in Fig. 7(f). This results in a complete closing of the second band gap, shown in Fig. 9(e), and the modes shift even further in opposite directions compared to Fig. 7(e). This approach of discretization can identify the extrema values of all the possible combinations of domains, to find the configuration with the largest change band gap width. With a finer discretization of the unit cell geometry, a possibly larger band gap shift could be obtained.

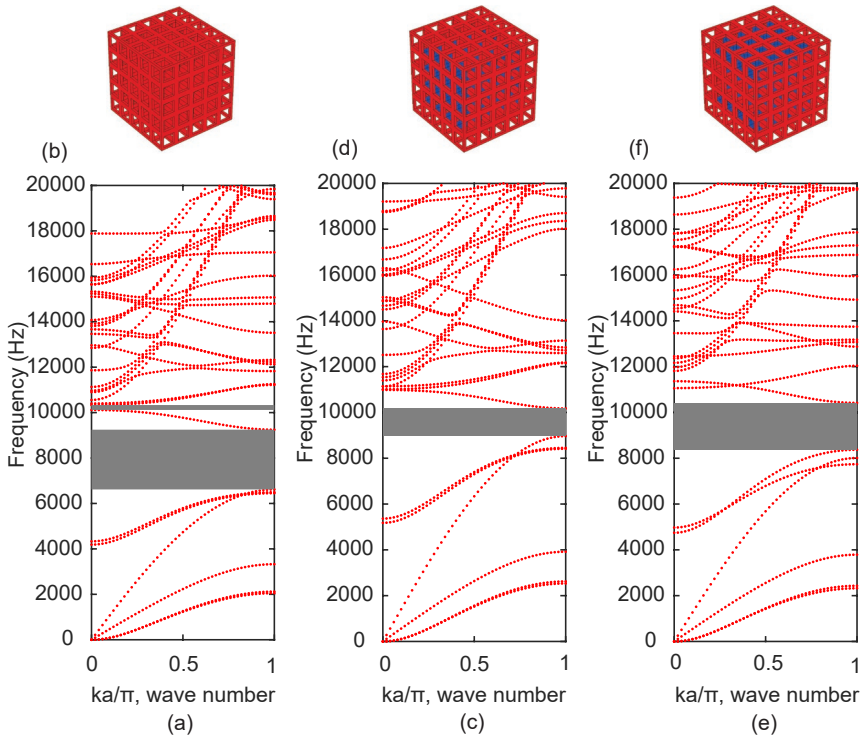

Figure 9: Results of thermal partitioning algorithm to decrease width of the first band gap (c,d), and close the second band gap (e,f): (a) Reference meta-structure dispersion relation of unit cell subjected to $140°C$. (c) Dispersion relation of lattice subjected to thermal partitioning shown in (d), where some domains (blue) are subjected to $-140°C$ and the rest of the lattice (red) is subjected to $140°C$. (e) Dispersion relation of lattice subjected to thermal partitioning shown in (f), where some domains (blue) are subjected to $-140°C$ and the rest of the lattice (red) is subjected to $140°C$.

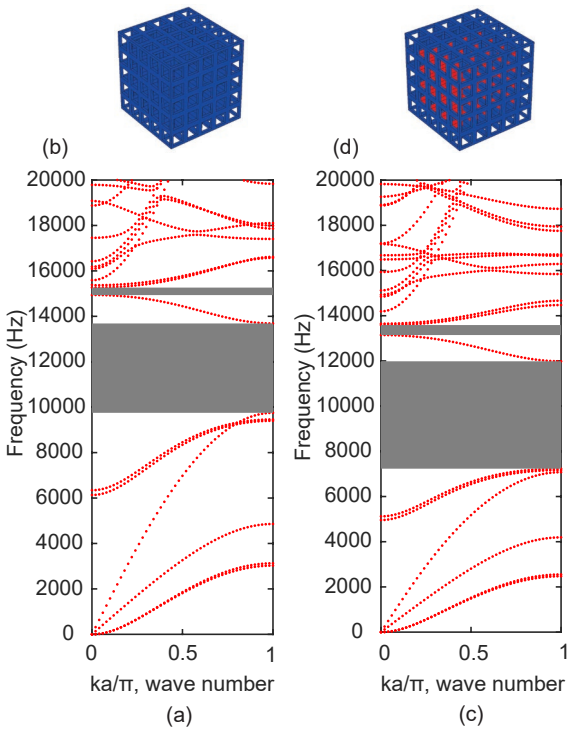

Figure 10: Results of thermal partitioning algorithm to widen the first band gap: (a) Reference meta-structure dispersion relation of (b) unit cell subjected to $-140°C$. (c) Dispersion relation of lattice subjected to thermal partitioning shown in (d), where some domains (red) are subjected to $140°C$ and the remaining domains (blue) are subjected to $-140°C$. The first band gap and second band gap have enhanced band gap widths as seen in (c) with values 49.4% and 3.3% respectively.

4 Thermally-induced geometry and stress effects on meta-structures

Other thermal effects on the meta-structures are related to its constituent materials thermal expansion coefficients: a temperature increase will cause an expansion and distortion of the meta-structure geometry due to a mismatch in thermal expansion coefficients between polycarbonate and steel. This mismatch will also induce thermal stresses within the meta-structure. An increase in the overall unit cell size of the meta-structure should cause a corresponding decrease in band gap frequency, since the frequency of Bragg-scattering induced band gaps scales inversely with the unit cell size. Prior work indicated the band gaps supported by the meta-structure studied here are indeed induced by Bragg scattering mechanisms [1]. All these effects, in addition to the change in material moduli, co-exist together. Here, we study the effects and their relative contribution to the band gaps of the meta-structure.

4.1 Contributions of geometric changes on band gaps

To study the change in geometry and dimensions of the meta-structure due to temperature, we consider a single unit cell. We apply a temperature change using finite element simulations (COMSOL Multiphysics) and allow the meta-structure unit cell to expand or contract, keeping the faces in the periodic direction flat as shown in Fig. 1(b) (see Sec. 3.1). The results of this simulation for an applied temperature of $-140°C$, shown in Fig. 12, demonstrate the thermal contraction of the meta-structure in all dimensions (Fig. 12a), as well as stresses induced in the meta-structure (Fig. 12b). The change in the overall unit cell dimensions due to the maximum thermal ex-

pansion or contraction is 0.9%.

We compare the dispersion curves of the meta-structure with only a change in modulus to dispersion curves with both the modulus and unit cell size change effects taken into account, Fig. 11. The unit cell length change causes a frequency shift of 21 Hz (0.18%) of the first band gap center frequency. This is negligible compared to frequency shift due to change in modulus values of 37.1% at this applied temperature. Even though the change is small, the change in unit cell size due to thermal expansion is considered in all the results shown in this work.

Other related negligible effects include the modulus change of the steel resonator by 6% from room temperature to $-140°C$ (from 205 GPa to 211.6 GPa) [24], since the resonator does not contribute to the stiffness of the modes. Further, an increase in unit cell size simultaneously leads to a decrease in density if the boundary conditions are considered free, however this also leads to a negligible frequency shift since the change in unit cell dimensions are less than 1%.

4.2 Influence of thermal stress on meta-structure

The applied temperature induces a small amount of thermal stress throughout most of the meta-structure since it is free to expand or contract, see Fig. 12(b). However, at the interface of the polycarbonate lattice and steel resonator there are high thermal stresses, with a maximum value in the polycarbonate of around 120.6 MPa von Mises stress, within a thin layer of the polycarbonate layer that interfaces with the steel for the applied temperature of $-140°C$. Higher stresses around 266.6 MPa are concentrated in the steel resonator. In the high temperature case, the maximum stress in the

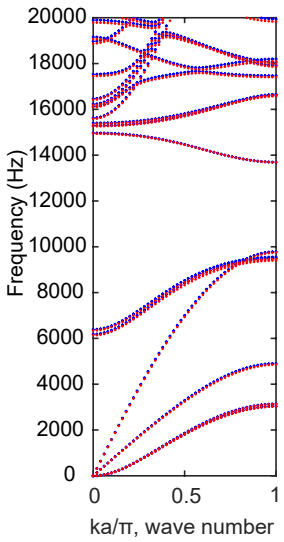

Figure 11: Dispersion curves that account for both change in modulus and unit cell size (represented by a circle marker) and for only a change in modulus (represented by a Plus sign marker).

polycarbonate is 58.58 MPa and the maximum stress in the steel is 96.94 MPa. While these high stresses are partially due to the mismatch in thermal expansion coefficients, they likely include artifacts from the numerical method due to stress concentrations at the corner of the steel resonator, which may be non-physical. In a physical system, these stresses may induce failure in the polycarbonate and at the polycarbonate-steel interface at the lowest temperatures studied here, since the stress in the polycarbonate exceeds its ultimate tensile strength. However, analysis on thermal stress effects in finite meta-structures show smaller stresses at this interface when the meta-structure ends are held fixed (see Sec. 5). Still, the large temperature ranges studied in this work may not be practical for this specific polycarbonate-steel meta-structure. However, these results could readily be implemented in meta-structure consisting of other materials with actuated moduli (e.g. shape memory alloys, or magneto-elastic materials).

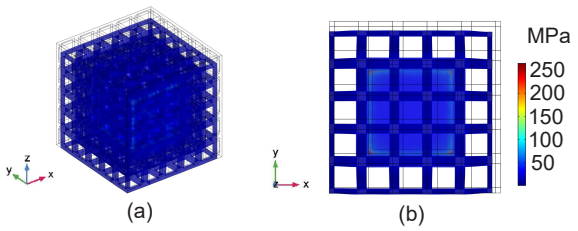

Figure 12: (a) Results of thermal simulation with applied temperature of $-140°C$, illustrating contracted unit cell with thermally-induced stresses plotted spatially. (b) von Mises stress (with units MPa) due to mismatch of thermal expansion coefficients between polycarbonate (lattice) and steel (resonator), plotted on the deformed unit cell. The wireframe illustrates the unit cell geometry at room temperature, and the solid structure illustrates the deformed geometry at applied temperature of $-140°C$.

5 Numerical validations with finite meta-structures

To numerically validate the band gaps in infinitely periodic meta-structures subjected to thermal tuning, we numerically analyze finite length meta-structures consisting of six-unit cells (Fig. 13) using COMSOL Multiphysics. On either ends of the lattice we add a 0.55mm thick plate on which to apply a uniform harmonic displacement, consistent with prior work [1]. We compare the vibration transmission response of the finite meta-structures to the band gap behavior numerically calculated in infinite meta-structures.

We first test the boundary condition of enforcing flat faces along the direction of periodicity in the dispersion analysis. To test this, we first subject the finite meta-structure to thermal expansion, ensuring flat faces only on the boundaries where loads are applied; note all other faces are free to expand, contract, or deform. We export the deformed mesh after this thermal expansion step, and then subject this deformed structure to frequency domain analysis. We keep one end fixed and subject the other to a harmonic displacement along the x-direction (direction of periodicity) in range of 0-20 kHz. The transmission is calculated as the ratio of reaction force on the fixed end of the meta-structure and the applied force.

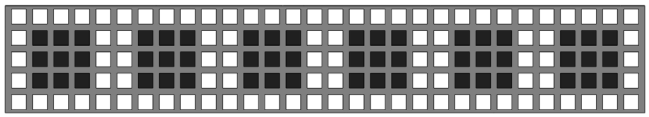

Figure 13: CAD model of 6-unit cell finite meta-structure

The vibration transmission for 6-unit cell meta-structures are shown in Fig. 14(a,b,c) at room temperature, $-140°C$, and a thermal partitioned example (corresponding to Fig. 8(e,f)), respectively. For the room temperature case, a range of minimized transmission is shown between 7,350 Hz and 12,750

Hz, which is in good agreement with band gap calculated from the dispersion analysis, between 7,133 Hz and 9,987 Hz. In the finite FEM, the excitation is along the x-direction. Modes that have displacement along the x-direction are preferentially excited, which explains the higher upper edge mode seen in finite meta-structure simulations that corresponds to the higher axial mode. This was calculated in previous work and validated experimentally [1]. Minimized transmission for $-140°C$ meta-structure was calculated to be between 10,000 Hz and 17,350 Hz, which is in good agreement with the corresponding band gap from the dispersion analysis, between 9,752 Hz and 13,686 Hz (Fig. 3(a)). Minimized transmission for the thermal partitioned example is similarly in good agreement to the calculated band gap. Overall, these results provide confidence that the boundary conditions applied in the infinite meta-structure analysis provides accurate results for finite meta-structures.

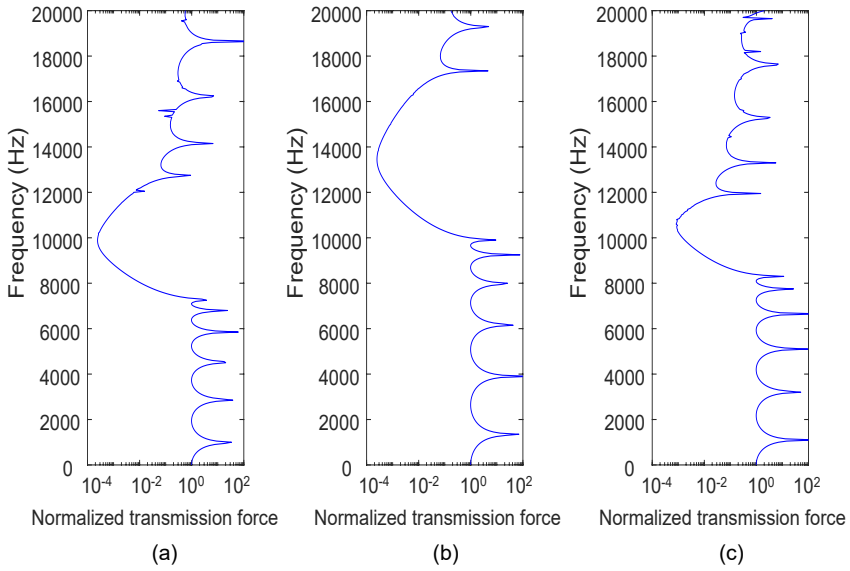

Figure 14: Normalized vibration transmission for 6-unit cell meta-structure at (a) room temperature [1], (b) $-140°C$, and (c) thermal partitioned as in Fig. 8(e,f).

To explore effects of thermal stress induced by the applied temperature

change, we do a pre-stressed frequency domain analysis on the structure shown in Fig. 13 to account for shift in frequencies due to internal thermal stresses. A similar analysis was previously done elsewhere [15]. The meta-structure is held in place using fixed boundary condition on both faces. The structure is subjected to an applied temperature of $-140°C$, and the thermal stresses that develop are considered as the initial state for the frequency domain step. The results of this thermal step are shown in Fig. 15(a), where the von Mises stress is superimposed on the finite meta-structure geometry; note the highest thermal stress in the polycarbonate is 84.7 MPa, and the maximum in the steel is 118.7 MPa. For the case where the finite meta-structure is subjected to an applied temperature of $140°C$, the maximum stress in the polycarbonate is 29 MPa and in the steel resonator is 41.4 MPa. So, in the high temperature case, the entire meta-structure remains in the elastic range, while the lowest temperature case there may be failure and/or delaminations in the polycarbonate.

The difference in the maximum stress at both $140°C$ and $-140°C$ compared to those calculated and shown in Fig. 12(a) is likely because the finite meta-structure in Fig. 15(a) is fixed at either end, thus preventing full expansion of the polycarbonate lattice. This induces some thermal stress throughout the entire meta-structure as opposed to the thermal stresses being concentrated at the interface of the steel and polycarbonate. The pre-stressed vibration transmission results for the finite meta-structure with applied temperature of $-140°C$ is shown in Fig. 15(b), along with the vibration transmission of the same meta-structure with undeformed geometry and devoid of any stresses. An applied decrease in temperature shifts the band gap center upwards by 275 Hz as shown in Fig. 15(b). A decrease in temperature will lead to a decrease in cross-sectional area, shifting the frequency down-

wards whereas the tensile thermal stresses developed due to constraints lead to stress hardening, thereby shifting the frequency upwards. In this specific case, the combination of these effects cause the frequency of the modes to increase. In the high temperature pre-stressed study the modal frequencies would shift downwards due to stress softening.

The thermal stress and length scale effects were here studied independently in FEM simulations. Numerical results on finite meta-structures show that the effects from thermal expansion and thermally-induced stresses have competing effects in terms of the frequency response of the meta-structure. However, both these effects cause insignificant shift in frequencies compared to the shift in band gaps due to change in lattice material modulus.

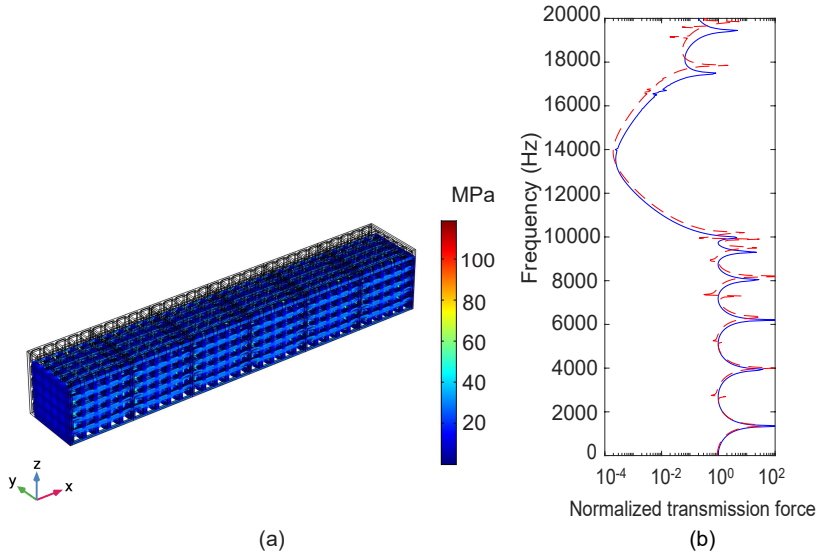

Figure 15: (a) Thermally expanded structure indicating von Mises stress with units of MPa. Black edges indicate the undeformed structure at room temperature. (b) Vibration transmission of a finite meta-structure with six unit cells subjected to a temperature of $140°C$ with deformed (dashed line) and without deformed geometry (solid line).

6 Prestressed and Mesh sensitivity Analysis in COMSOL

To understand how frequencies change with temperature, we consider a simple beam, Fig. 16, with dimensions 10mm x 1mm x 1mm and do a Prestressed analysis in COMSOL. Built-In material "Steel AISI 4340", from COMSOL material library was used to model the beam. An eigenfrequency study of this beam indicates the existence of the first longitudinal mode at 128081.5 Hz. We apply a harmonic load along the longitudinal direction and the resonance peak is in close agreement with the modal frequency obtained from eigenfrequency study as seen in Fig. 17.

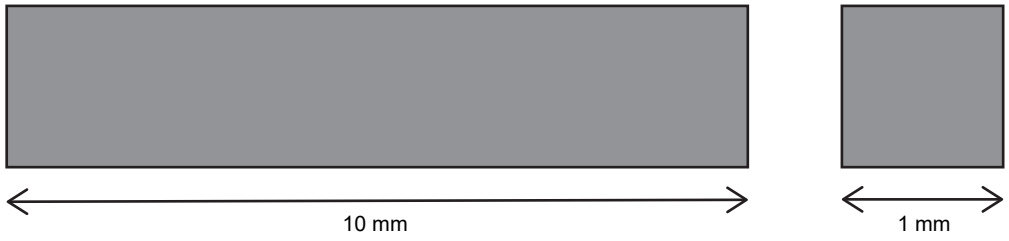

Figure 16: Cantilever beam having a square cross-section with dimensions 10mm x 1mm x 1mm.

We subject the beam to temperature change, ΔT=100K, keeping one end fixed allowing free thermal expansion subjecting the structure. The deformed structure is exported and the new density value is calculated by applying conservation of mass. Eigenfrequency analysis of the thermally expanded structure is shown in Fig. 17 and is found to be 128159.6 Hz. Using "Prestressed Eigenfrequency" analysis the longitudinal mode is found at 128160.3 Hz compared to the deformed structure analysis of 128159.6 Hz. This small error can be attributed to different meshing of the thermally expanded (deformed) and original structures. A finer mesh size will bring the difference even

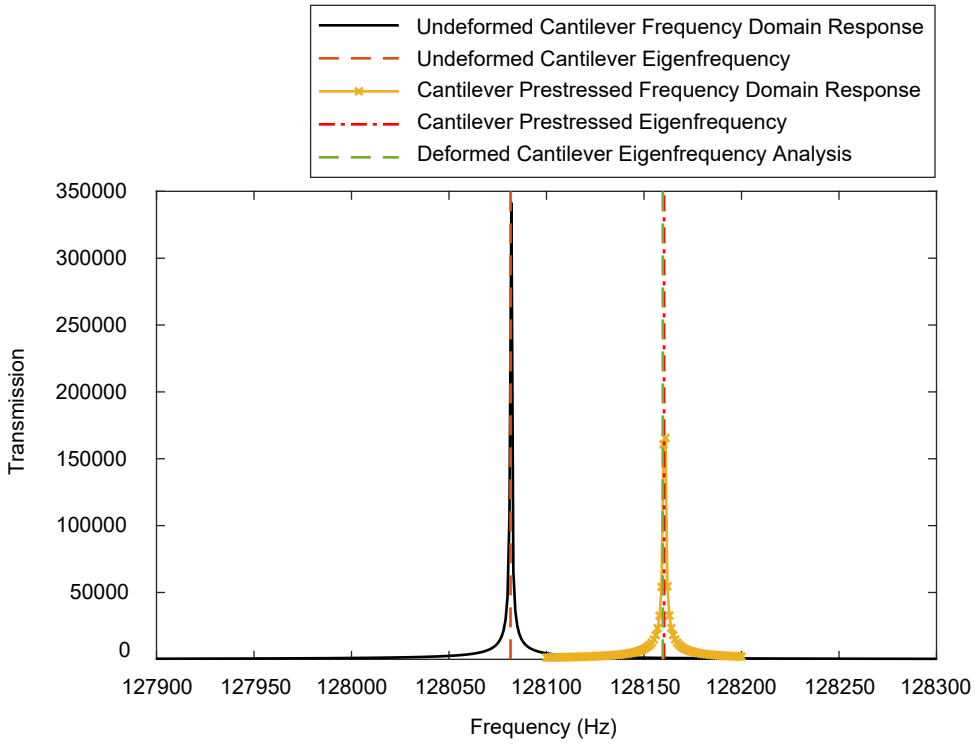

Figure 17: Transmission plots of undeformed cantilever beam and cantilever beam subjected to a temperature change, ΔT=100K. Also indicated is the eigenfrequency of the undeformed beam and the thermally expanded beam. The eigenfrequency of the thermally expanded beam is calculated using two different methods, first by exporting the deformed structure and second using Prestressed Eigenfrequency study in COMSOL

lower. The frequency of the longitudinal mode is proportional to $\sqrt{EA/L}$. When subjected to a temperature change, the frequency is proportional to $\sqrt{1+\alpha\Delta T} = \sqrt{1+12.3*10^{-6}*100} = 1.000614811$. Therefore the analytically predicted eigenfrequency when subjected to thermal expansion is $128081.5 * 1.000614811 = 128160.246$. The predicted and computed results are in very close agreement. A Prestressed frequency domain analysis is performed and the peak in transmission is in close agreement with the calculated eigenfrequencies. For transmission plots it is accurate to use surface integration of reaction force(solid.RFx) than a surface integration of trac-

tion(solid.Tax).

In order to do a constrained thermal analysis the reference point in thermal expansion step should be set to the coordinates of the plane of constraint as shown in Fig. 18. Compressive thermal stresses will shift the frequencies lower because of stress softening and tensile stresses will move the frequencies higher due to stress hardening.

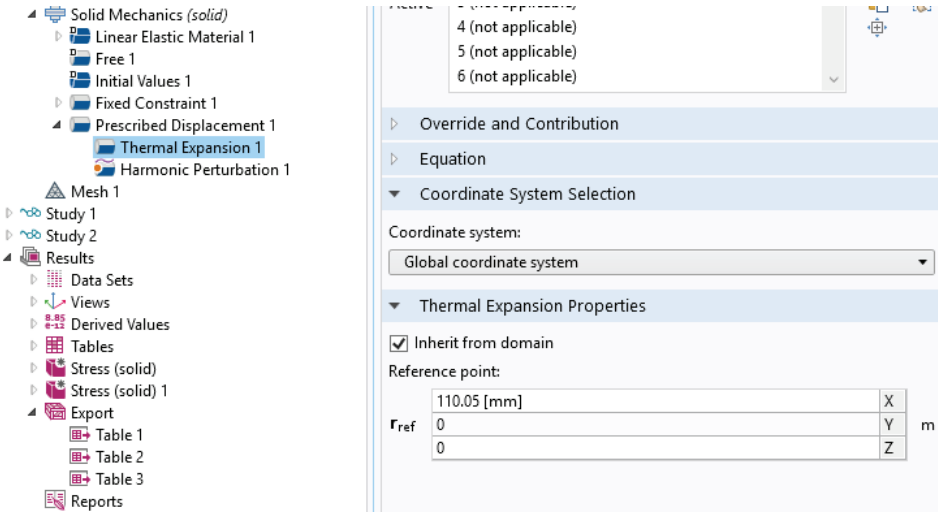

Figure 18: The reference point coordinates should be set to the location of "Prescribed Displacement" face

A mesh sensitivity analysis was performed in order to check the convergence of the finite element solution. The convergence plots for the first 16 modes are shown in Fig. 19, where the x-axis indicates the degrees of freedom and y-axis represents the % error. The highest degrees of freedom corresponding to a minimum maximum element size was chosen as the reference and error at higher maximum element sizes was calculated with respect to this reference. A maximum element size of 0.74mm was chosen to have sufficiently large degrees of freedom.

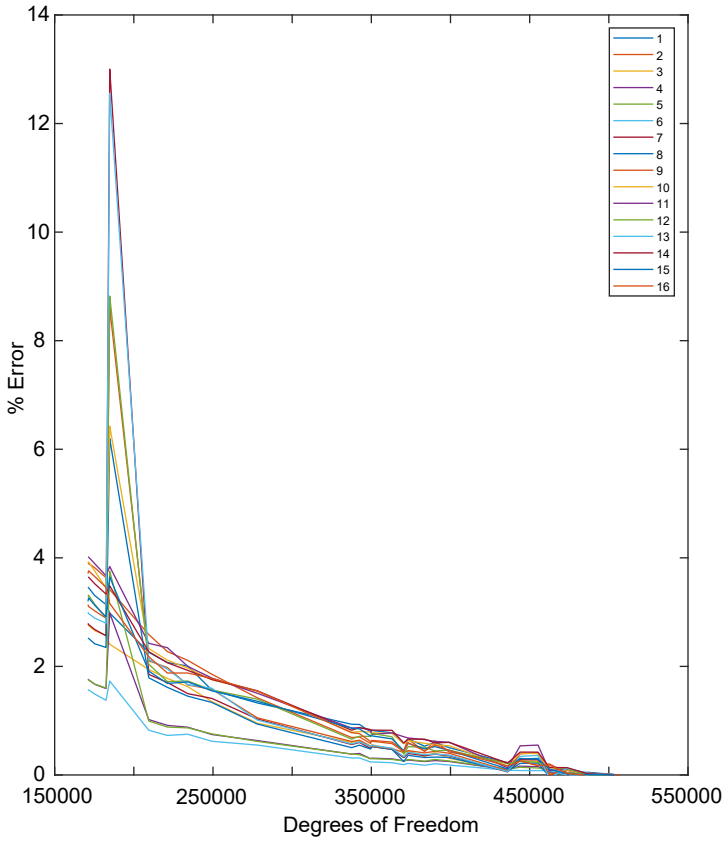

Figure 19: Sensitivity analysis results of the first 16 eigenfrequencies are shown. The maximum degrees of freedom is set as the reference to measure the % error. For the eigenfrequency analysis, the chosen element size resulted in degrees of freedom slightly more than 500,000.

7 Conclusions

We have demonstrated tunability of band gaps in lattice-resonator meta-structures using an applied temperature. Global changes in temperature of the entire meta-structure shift all the modes equally in the frequency spectrum, whereas thermal partitioning enables partial opening and closing of band gaps. Subjecting the structure to thermal partitioning gives greater control of individual modes.

The meta-structure band gap properties are only shown numerically here, and prior work has experimentally validated these meta-material band gaps at room temperature [1]. While experimental validations of global temperature tuning presented here could be realized, thermal stresses induced at the boundary of lattice and resonator due to the mismatch in thermal expansion coefficients between polycarbonate and steel may cause delaminations at the interface of the polycarbonate and steel. The temperatures studied are also somewhat impractical for polycarbonate material, and the stability of the structure may be questionable around the glass transition temperature of polycarbonate. Further, thermal partitioning would be very difficult to achieve experimentally, given that beams within a few millimeters of each other would need to be drastically different temperatures. However, these concepts and results provide a platform that could be successfully applied to other materials that induce a modulus change upon external application, for example shape memory alloys or magneto-elastic materials.

References

[1] K. H. Matlack, A. Bauhofer, S. Krödel, A. Palermo, C. Daraio, Composite 3D-printed meta-structures for low frequency and broadband vibration absorption, PNAS 113 (30) (2015) 8386–8390. doi:10.1073/pnas.1600171113.

[2] M. I. Hussein, M. J. Leamy, M. Ruzzene, Dynamics of Phononic Materials and Structures: Historical Origins, Recent Progress, and Future Outlook, Applied Mechanics Reviews 66 (4) (2014) 040802. doi:10.1115/1.4026911.

[3] P. A. Deymier (Ed.), Acoustic Metamaterials and Phononic Crystals, Vol. 173, Springer, Berlin, 2013.

[4] M.-H. Lu, L. Feng, Y.-F. Chen, Phononic crystals and acoustic metamaterials, Materials Today 12 (12) (2009) 34–42. doi:10.1016/S1369-7021(09)70315-3.

[5] J. B. Berger, H. N. G. Wadley, R. M. McMeeking, Mechanical metamaterials at the theoretical limit of isotropic elastic stiffness, Nature 543 (2017) 533–537. doi:10.1038/nature21075.

[6] X. Zheng, H. Lee, T. H. Weisgraber, M. Shusteff, J. DeOtte, E. B. Duoss, J. D. Kuntz, M. M. Biener, Q. Ge, J. A. Jackson, S. O. Kucheyev, N. X. Fang, C. M. Spadaccini, Ultralight, Ultrastiff Mechanical Metamaterials, Science 344 (6190) (2014) 1373–1377. doi:10.1126/science.1252291.

[7] S. Babaee, N. Viard, P. Wang, N. X. Fang, K. Bertoldi, Harnessing Deformation to Switch On and Off the Propagation of Sound, Advanced Materials 28 (8) (2016) 1631–1635. doi:10.1002/adma.201504469.

[8] K. Bertoldi, M. C. Boyce, Mechanically triggered transformations of phononic band gaps in periodic elastomeric structures, Physical Review B 77 (5) (2008) 052105. doi:10.1103/PhysRevB.77.052105.

[9] Y. Chen, T. Li, F. Scarpa, L. Wang, Lattice Metamaterials with Mechanically Tunable Poisson's Ratio for Vibration Control, Physical Review Applied 7 (2) (2017) 024012. doi:10.1103/PhysRevApplied.7.024012.

[10] N. Boechler, J. Yang, G. Theocharis, P. G. Kevrekidis, C. Daraio, Tunable vibrational band gaps in one-dimensional diatomic granular crystals with three-particle unit cells, Journal of Applied Physics 109 (7) (2011) 074906. doi:10.1063/1.3556455.

[11] Y. Cheng, X. J. Liu, D. J. Wu, Temperature effects on the band gaps of Lamb waves in a one-dimensional phononic-crystal plate (L), The Journal of the Acoustical Society of America 129 (3) (2011) 1157–1160. doi:10.1121/1.3543970.

[12] K. L. Jim, C. W. Leung, S. T. Lau, S. H. Choy, H. L. W. Chan, Thermal tuning of phononic bandstructure in ferroelectric ceramic/epoxy phononic crystal, Applied Physics Letters 94 (19) (2009) 193501. doi:10.1063/1.3136752.

[13] Y. Yao, F. Wu, X. Zhang, Z. Hou, Thermal tuning of Lamb wave band structure in a two-dimensional phononic crystal plate, Journal of Applied Physics 110 (12) (2011) 123503. doi:10.1063/1.3669391.

[14] H. Sadeghi, A. Srivastava, A. Amirkhizi, S. Nemat-Nasser, Acoustic Filter Design Using Temperature Tuning, Proceedings of the American Society for Composites - 31st Technical Conference, ASC 2016arXiv:1611.10005.

[15] Y. Wu, K. Yu, L. Yang, R. Zhao, X. Shi, K. Tian, Effect of thermal stresses on frequency band structures of elastic metamaterial plates, Journal of Sound and Vibration 413 (2018) 101–119. doi:10.1016/j.jsv.2017.10.014.

[16] M. Thota, S. Li, K. W. Wang, Lattice reconfiguration and phononic band-gap adaptation via origami folding, Physical Review B 95 (6) (2017) 064307. doi:10.1103/PhysRevB.95.064307.

[17] C. Goffaux, J. P. Vigneron, Theoretical study of a tunable phononic band gap system, Physical Review B 64 (7) (2001) 075118. doi:10.1103/PhysRevB.64.075118.

[18] A. Nanda, M. A. Karami, Tunable bandgaps in a deployable metamaterial, Journal of Sound and Vibration 424 (2018) 120–136. doi:10.1016/j.jsv.2018.03.015.

[19] L.-Y. Wu, M.-L. Wu, L.-W. Chen, The narrow pass band filter of tunable 1D phononic crystals with a dielectric elastomer layer, Smart Materials and Structures 18 (1) (2009) 015011. doi:10.1088/0964-1726/18/1/015011.

[20] Z. Chen, C. Xue, L. Fan, S.-y. Zhang, X.-j. Li, H. Zhang, J. Ding, A tunable acoustic metamaterial with double-negativity driven by electromagnets, Scientific Reports 6 (2016) 30254. doi:10.1038/srep30254.

[21] F. Allein, V. Tournat, V. E. Gusev, G. Theocharis, Tunable magneto-granular phononic crystals, Applied Physics Letters 108 (16) (2016) 161903. doi:10.1063/1.4947192.

[22] J.-F. Robillard, O. Bou Matar, J. O. Vasseur, P. A. Deymier, M. Stippinger, A.-C. Hladky-Hennion, Y. Pennec, B. Djafari-Rouhani, Tunable magnetoelastic phononic crystals, Applied Physics Letters 95 (12) (2009) 124104. doi:10.1063/1.3236537.

[23] R. L. Harne, Z. Deng, M. J. Dapino, Adaptive magnetoelastic metamaterials: A new class of magnetorheological elastomers, Journal of Intelligent Material Systems and Structures 29 (2) (2018) 265–278. doi:10.1177/1045389X17721037.

[24] W. E. Luecke, J. D. McColskey, C. N. McCowan, S. W. Banovic, R. J. Fields, T. Foecke, T. A. Siewert, F. W. Gayle, Mechanical Properties of Structural Steels, Tech. rep., NIST NCSTAR 1-3D (2005).

[25] P. Cornwell, S. W. Doebling, C. R. Farrar, Application of the strain energy damage detection method to plate-like structures, Journal of Sound and Vibration 224 (2) (1999) 359–374. doi:10.1006/JSVI.1999.2163.

[26] F. Seguel, V. Meruane, Damage assessment in a sandwich panel based on full-field vibration measurements, Journal of Sound and Vibration 417 (2018) 1–18. doi:10.1016/j.jsv.2017.11.048.

[27] Z. Y. Shi, S. S. Law, L. M. Zhang, Structural damage localization from modal strain energy change, Journal of Sound and Vibration 218 (5) (1998) 825–844. doi:10.1006/jsvi.1998.1878.